3 July 2025, Preprint v2 · CC-BY 4.0 Qeios

Research Article

Active Matter Flocking via Predictive Alignment

Julian Giraldo-Barreto[1], **Viktor Holubec**[1]

1. Department of Macromolecular Physics, Faculty of Mathematics and Physics, Charles University, Prague, Czech Republic

Understanding collective self-organization in active matter, such as bird flocks and fish schools, remains a grand challenge in physics. Interactions that induce alignment are essential for flocking; however, alignment alone is generally insufficient to maintain group cohesion in the presence of noise, leading traditional models to introduce artificial boundaries or explicit attractive forces. Here, we propose a model that achieves cohesive flocking through purely alignment-based interactions by introducing predictive alignment, in which agents reorient to maximize alignment with the prevailing orientations of their anticipated future neighbors. Implemented in a discrete-time Vicsek-type framework, this approach delivers robust, noise-resistant cohesion without additional parameters. In the stable regime, flock size scales linearly with interaction radius, remaining nearly immune to noise or propulsion speed, and the group coherently follows a leader under noise. These findings reveal how predictive strategies enhance self-organization, paving the way for a new class of active matter models blending physics and cognitive-like dynamics.

Corresponding authors: Julian Giraldo-Barreto, julian.giraldob@matfyz.cuni.cz; Viktor Holubec, viktor.holubec@matfyz.cuni.cz

Introduction

From micrometer-sized bacteria to complex animals, biological organisms sense their environment, process directional cues, and adapt their motion accordingly [1][2][3]. Similar feedback mechanisms are also indispensable in the control of autonomous robotic systems [4]. Based on visual [5], acoustic [6], or chemical [7] signals, these perception-reaction interactions result in the self-organization of large ensembles of cognitive individuals into cohesive spatiotemporal patterns, such as bird flocks [8], fish schools [9], and human crowds [10]. The study of these collective behaviors falls within the domain of active matter physics [3][11][12]. Models of collective behavior in active matter span Reynolds-type ‘boid’ models [13], Vicsek-type

doi.org/10.32388/MCG19T.2

‘alignment’ models [14][15][16], Couzin-type ‘zonal’ models [17], ‘vision cone’ models [18][19], motivation-based models [20][21][22][23], vision-based models [5][24][25], energy-efficiency models [26], and other biologically motivated models [27], as well as models designed for controlling robotic swarms [28].

Vicsek-type models that rely solely on alignment interactions struggle to maintain cohesion without artificial mechanisms such as periodic or reflecting boundaries, or additional attractive forces [29][30]. However, boundary conditions can influence bulk behavior, especially in the parameter regime associated with microphase separation, where density waves tend to align with the symmetries of the periodic simulation box [29][30][31]. Similarly, incorporating attractive interactions can induce swirling motion [32], which was absent in the original model. Other models achieve cohesion through either direct attractive interactions [33] or explicit mechanisms, such as active or passive reorientation and movement toward a local or global center of the group [13][17][18][19]. Notable exceptions include models where cohesion is not explicitly built into the algorithm, such as the maximum path entropy model [22][23] or vision-based models [5]. However, these approaches do not restrict the agents’ sight range, effectively introducing long-range interactions. To our knowledge, no prior model achieves cohesive flocking with purely alignment interactions over a finite range.

Here, we introduce predictive alignment in a Vicsek-type framework with a limited interaction radius ζ. We interpret the alignment interactions as biologically motivated social behaviors based on individual decision-making. Specifically, we implement them using the sociological rule of “copy the other” [34], whereby an individual adopts the prevailing state of its neighbors—a strategy known to enhance individual success within a group.

Our model reduces to a variation of the Vicsek model for simple agents that cannot anticipate future positions. However, agents capable of anticipating their future neighbors effectively optimize a trade-off between alignment and proximity. This yields a cohesive flocking model based solely on alignment with the prevailing orientation of neighbors, without the need for additional parameters or boundary constraints. The system undergoes a dynamical transition to an incoherent state with increasing noise and distance traveled per timestep over the interaction radius. In the flocking state, the stationary flock radius is comparable to the interaction radius, independent of agent speed, and increases linearly with noise—albeit with a very small slope. Additionally, the group efficiently follows a subgroup of maneuvering leaders. Our results reveal how predictive strategies enable robust self-organization akin to natural systems.

Model

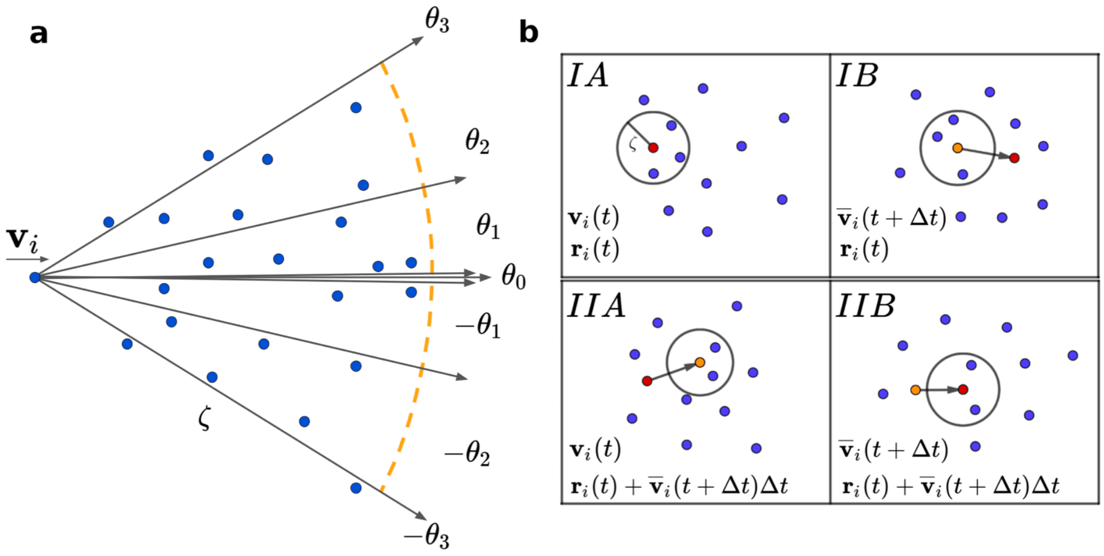

Figure 1. Model.a At each discrete time step, individual agents aim to align as closely as possible with the prevailing orientation of their neighbors within a circle of radius ζ. To achieve this, they select one of seven possible reorientations, $\Delta\theta_i^t \in \Omega_\theta = \pm\{0, 0.01, 0.2, 0.5\}$, that maximizes the correlation function in Eq. (3). All agents update their orientation in parallel. **b** We implemented four different strategies (IA–IIB) for evaluating the correlation function. In strategies I, the correlation is computed using the current neighbors ($\mathbf{r}_i = \mathbf{r}_i(t)$), whereas in strategies II, it is computed using predicted future neighbors [$\mathbf{r}_i = \mathbf{r}_i(t) + \overline{\mathbf{v}}_i(t+\Delta t)\Delta t$], as illustrated by the black circles. In strategies A, the agent's own orientation is included inside the bracket of the correlation function ($\mathbf{v}_i = \mathbf{v}_i(t)$), introducing orientational inertia, which is absent in strategies B ($\mathbf{v}_i = \overline{\mathbf{v}}_i(t+\Delta t)$).

Biological active agents in nature follow evolutionarily adapted instincts and, in the case of higher animals, sometimes even learned or cognitively driven strategies to achieve specific goals such as collision avoidance or foraging. Similar mechanisms are also implemented in the development of autonomous robotic systems. These strategies are shaped by physical, biological, or technical constraints, which limit the range of possible dynamical and adaptive responses. We consider a system of N Vicsek-type agents self-propelling in discrete time in two dimensions with a constant velocity v_0 in the direction of their orientation vectors $(\cos\theta_i^t, \sin\theta_i^t)$, $i = 1, \ldots, N$. At each discrete time step t, the agents reorient by discrete angles $\Delta\theta_i^t \in \Omega_\theta = \pm\{0, 0.01, 0.2, 0.5\}$ rads to achieve maximum alignment with their neighbors, as shown in Fig. 1a. We used a discrete set of angles mainly for computational efficiency—selecting the optimal reorientation from a small, predefined set is significantly faster than solving the corresponding continuous optimization problem. The set Ω_θ is chosen to allow agents to reorient either gradually or sharply, depending on how far their desired direction deviates from their current heading, to mimic the original Vicsek model. Nevertheless, as shown in Sec. S8 [1], a variant of the model with only three possible reorientation angles yields qualitatively similar results. The limited reorientation can be interpreted as a realistic constraint, reflecting the physical limitations of actual agents, such as friction or biomechanical restrictions that prevent abrupt turns. We also note that in the IIA and IIB variants of the model, discussed below and in Fig. 1b, the discrete angle sets effectively define agent's field of view.

The imperfections in reorientation of the agents are reflected by a noise term ξ_i^t sampled from the interval $\eta[-\pi, \pi]$, added to the chosen $\Delta\theta_i^t$. The resulting dynamical equations for ith particle position $\mathbf{r}_i^t$ and velocity $\mathbf{v}_i^t$ are given by:

$$\mathbf{r}_i^{t+\Delta t} = \mathbf{r}_i^t + \mathbf{v}_i^{t+\Delta t}\Delta t, \tag{1}$$

$$\theta_i^{t+\Delta t} = \theta_i^t + \Delta\theta_i^t + \xi_i^t, \tag{2}$$

What remains is to choose a strategy to determine the reorientation angle $\Delta\theta_i^t$ in Eq. (2). In the classical discrete-time Vicsek model, $\Delta\theta_i^t$ is chosen to align the ith agent's velocity with the average velocity $\mathbf{V}_i^t$ of its neighbors. To incorporate this effect, we define $\Delta\theta_i^t = \arg\max_{\Delta\theta_i} C_i^t$, i.e., as the argument that maximizes the correlation function

$$C_i^t = \overline{\mathbf{v}}_i^{t+\Delta t} \cdot \left(\sum_{j=1}^{N} H\left(|\mathbf{r}_i - \mathbf{r}_j^t| - \zeta \right) \mathbf{v}_j^t - (\mathbf{v}_i^t - \mathbf{v}_i) \right). \tag{3}$$

It can be interpreted as the correlation between the agent's future desired velocity, $\overline{\mathbf{v}}_i^{t+\Delta t} = v_0 \left[\cos(\theta_i^t + \Delta\theta_i^t), \sin(\theta_i^t + \Delta\theta_i^t)\right]$, and the generalized, non-normalized average velocity of its predicted future neighbors within the interaction radius centered at its predicted future position $\mathbf{r}_i$ (see Fig. 1b). Since C_i^t is not normalized, it quantifies the degree of alignment between the ith agent's intended future heading and the prevailing orientation of its predicted future neighbors. Thus, it serves as a natural objective function to maximize by agents aiming to 'copy' the prevalent orientation of their neighbors. The Heaviside step function H is modified such that $H(0) = 1$, ensuring that C_i^t properly accounts for all particles within the interaction radius ζ. Depending on the cognitive abilities of the agents, the predicted velocity $\mathbf{v}_i$ and position $\mathbf{r}_i$ used in the non-normalized average velocity in Eq. (3) can be evaluated either at time t—for agents unable to predict their future state—or at time $t + \Delta t$—for cognitively more capable agents. This results in four distinct ways to define the correlation, as illustrated in Fig. 1b. In principle, perceptual errors in real-world agents would necessitate the inclusion of a noise term within the bracket in Eq. (3). However, we neglect such perceptual noise in the present study and, using the terminology of Vicsek model modifications, consider only angular noise while neglecting vectorial noise [35]. If C_i^t vanishes for all possible reorientations, the agent updates its orientation purely by noise, i.e., $\Delta\theta_i^t = 0$ in Eq. (2).

The strategies IA and IB calculate the correlation C_i^t with the current neighbors of the agent i, $\mathbf{r}_i = \mathbf{r}_i^t$. Strategy IA further takes the agent's current velocity $\mathbf{v}_i = \mathbf{v}_i^t$ inside the sum, and IB uses the interpolated velocity $\mathbf{v}_i = \overline{\mathbf{v}}_i^{t+\Delta t}$ instead. In both cases, $C_i^t = n_i^t \overline{\mathbf{v}}_i^{t+\Delta t} \cdot \mathbf{V}_i^t + C_0$, where C_0 is a constant, n_i^t the number of neighbors of agent i at time t and $\mathbf{V}_i^t$ their average velocity. For IA, $C_0 = 0$ and the agent i is counted in n_i^t and $\mathbf{V}_i^t$, so that $n_i^t = \sum_{j=1}^N H\left(|\mathbf{r}_i^t - \mathbf{r}_j^t| - \zeta\right)$ and $\mathbf{V}_i^t = \sum_{j=1}^N H\left(|\mathbf{r}_i^t - \mathbf{r}_j^t| - \zeta\right) \mathbf{v}_j^t / n_i^t$. For IB, $C_0 = v_0$ and the agent i is not counted in the definition of n_i^t and $\mathbf{V}_i^t$ ($j \neq i$ in the sums above). Nevertheless, in both cases, n_i^t and C_0 are independent of $\Delta\theta_i^t$ and thus the intended velocity that maximizes C_i^t is the one best aligned with the average velocity $\mathbf{V}_i^t$. Notably, considering the agent's own velocity in $\mathbf{V}_i^t$ introduces slight orientational inertia in IA, as agents take their own heading into account. These two strategies correspond to two variants of the Vicsek model: Vicsek model A, which includes the agent's own velocity in the average velocity calculation, and Vicsek model B, which does not (see Sec. S1 [1]).

The strategies IIA and IIB, use the neighbors corresponding to the intended future position of agent i at time $t + \Delta t$, $\mathbf{r}_i = \mathbf{r}_i^t + \overline{\mathbf{v}}_i^{t+\Delta t} \Delta t$, and thus require calculating the correlation C_i^t using different neighbors for each value of the realignment angle. From now on, we will call these two strategies predictive and the corresponding models as predictive models. As above, strategy IIA further takes the agent's current velocity $\mathbf{v}_i = \mathbf{v}_i^t$ inside the sum, and IIB the interpolated velocity $\mathbf{v}_i = \overline{\mathbf{v}}_i^{t+\Delta t}$. Also in these cases, $C_i^t = n_i^t \overline{\mathbf{v}}_i^{t+\Delta t} \cdot \mathbf{V}_i^t + C_0$. Nevertheless, the number of neighbors of i , n_i^t, and their average velocity, $\mathbf{V}_i^t$, are now calculated with respect to its intended position $\mathbf{r}_i(t) + \overline{\mathbf{v}}_i(t + \Delta t)\Delta t$ and thus they depend on the reorientation angle. For IIA the agent i is counted in n_i^t and $C_0 = 0$. For IIB, $C_0 = v_0$ and the agent i does not contribute to the averages. Importantly, in both these strategies, the optimal reorientation angle follows from a tradeoff balancing the number of nearest neighbors and alignment with the average velocity, resulting in an attractive alignment interaction. Different from IIB, IIA, in addition, has some positional inertia.

The time step Δt affects only the relaxation times and does not alter the stationary state. Upon rescaling particle positions by the interaction radius ζ, the stationary behavior of this model is controlled by two parameters: the ratio of the distance traveled per timestep to the interaction radius, $v_0 \Delta t / \zeta$, and the noise-induced orientation change per time step, quantified by η. In the following, we consider groups of $N = 200$ agents initially positioned randomly within a square of side length $L = 4\zeta$, with $\zeta = 1$ and $\Delta t = 1$. In Sec. S10 [1], we show that using a larger $N = 500$ produces qualitatively the same results. A more physically grounded, continuous-time variant of the model is described in Sec. S2 [1].

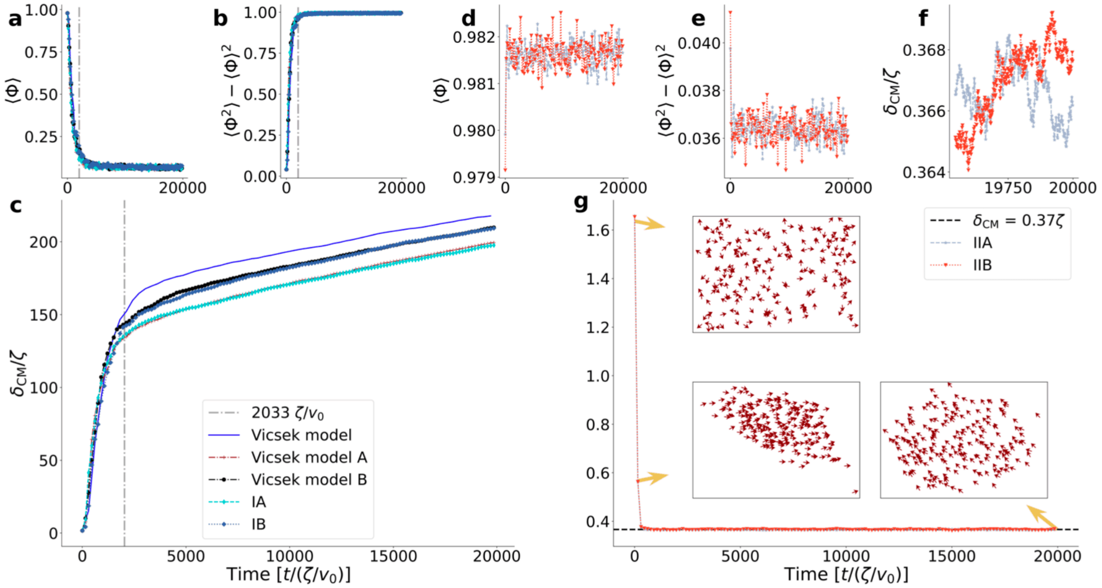

Figure 2. Comparison between Vicsek-like and predictive models. The agents started with uniformly distributed orientations and evolved according to the standard time-discrete Vicsek model, its modifications A and B (see Sec. S1 [1]), as well as the decision-based models IA–IIB defined in the main text. For all models, we set the reduced speed to $v_0/\zeta = 0.0076$, noise intensity to $\eta = 0.1$, and averaged the shown data over 25 replicas with different noise realizations. **a**–**c**, The Vicsek-type models exhibit a rapid loss of cohesion, indicated by **a** a sharp decrease in the average polarization $\langle \Phi \rangle$, **b** an increase in its fluctuation $\langle \Phi^2 \rangle - \langle \Phi \rangle^2$, and **c** a rapid growth of the average agent-to-center-of-mass distance, δ_{CM}. These effects occur before $t \approx 2033\zeta/v_0$, predicted from diffusive spreading analysis of Vicsek model (vertical dashed lines). **d**–**g**, The predictive models IIA and IIB yield nearly identical stable flocking behaviors, with **d** a consistently high average polarization fluctuating weakly around 0.98, **e** low polarization variance, and **f** a closely packed system configuration, where the average agent-to-center-of-mass distance fluctuates around 0.366. **g** The system size self-adjusts as the initially square-shaped flock transitions through an elongated intermediate state before settling into a final circular configuration (insets). The system size relaxation time, defined as the point when δ_{CM} drops to half of its initial value, is approximately $100\zeta/v_0$. Analogously defined relaxation times for $\langle \Phi \rangle$ and $\langle \Phi^2 \rangle - \langle \Phi \rangle^2$ are shorter than ζ/v_0 (see Sec. S7 [1]).

Models with purely alignment interactions, such as the Vicsek model, fail at maintaining group cohesion even under arbitrarily weak noise due to the diffusive spreading of agents. The time it takes for two particles, initially at the same position, to 'diffuse' further away than one interaction radius can be estimated as

$\left(\frac{1}{5}+\frac{3}{2\pi^2\eta^2}\right)\frac{\zeta^2}{v_0^2}$ (see Sec. S4 [1]). It is reasonable to expect that as the number of agents increases, the Vicsek flock will break up into subgroups more quickly. For $\eta=0.1$ and $v_0/\zeta=0.0076$ as used in Fig. 2, our estimate suggests that flock coherence is lost before $t\approx 2033\zeta/v_0$. For Vicsek-like models IA, IB, and for the standard Vicsek model, this prediction aligns remarkably well with the saturation point where (a) the average polarization, $\langle\Phi\rangle$, halts its rapid decrease, and (b) the polarization variance, $\langle\Phi^2\rangle-\langle\Phi\rangle^2$, halts its rapid increase. It also marks the end of the initial sharp rise in the average agent-to-center-of-mass distance, δ_{CM} (c). Beyond this point, the system size expands ballistically as the single flock fragments into multiple sub-flocks, indicated by the vanishing polarization and peak variance in (a) and (b). (For precise definitions of the order parameters, see Sec. S3 [1].) On the other hand, the predictive models IIA and IIB produce highly polarized, closely packed, and coherent flocks, with a self-adjusted $\delta_{\mathrm{CM}}\approx 0.4\zeta$, corresponding to a flock radius of approximately 0.6ζ. This implies that the entire stationary flock fits within a single interaction radius, making the model unrealistic from a biological perspective, where the number of perceived neighbors is limited [8]. The corresponding order parameters exhibit only minor fluctuations and remain stable over time—at least over the simulation durations we tested, which span up to ten diffusive spreading times.

Noise induced dynamical transition

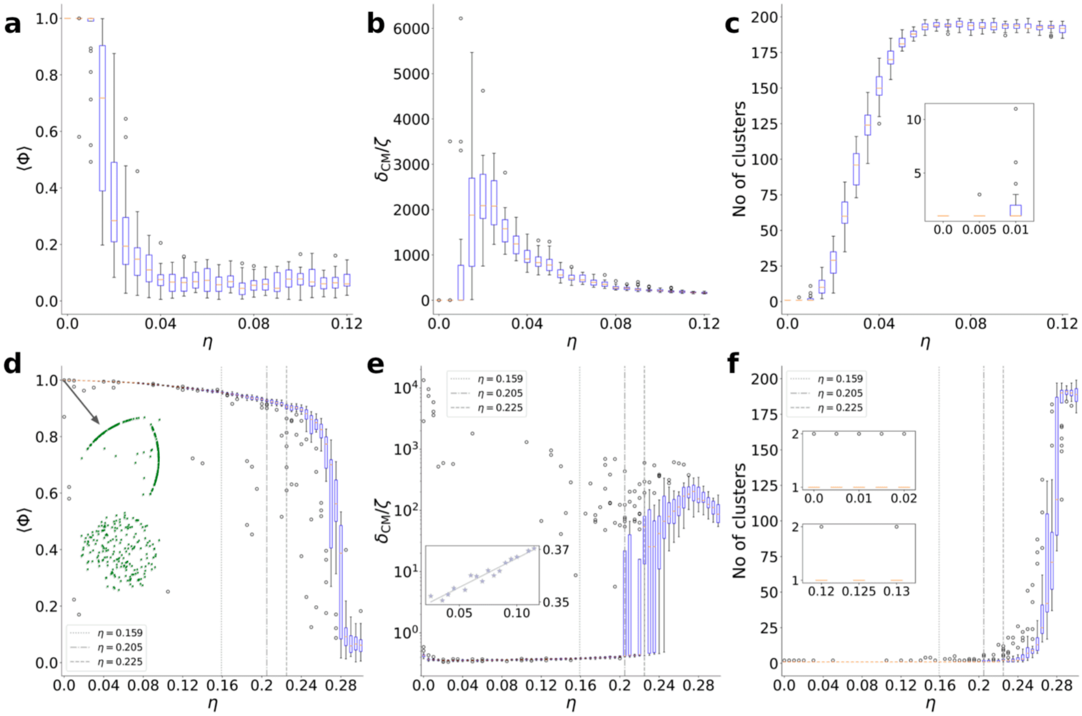

Figure 3. Effects of noise in Vicsek model and the predictive model IIA. Boxplots represent results from 25 independent simulations with different noise realizations, where orange lines indicate the median, boxes span the interquartile range, whiskers extend to data points within 1.5 times the interquartile range, and outliers are shown as individual circles. **a–c** In the Vicsek model, for noise levels $\eta \gtrapprox 0.005$, flock cohesion is lost, with fragmentation increasing at higher noise levels, as reflected by **a** reduced average polarization $\langle \Phi \rangle$, **b** an increased average agent-to-center-of-mass distance δ_{CM}, and **c** a greater number of clusters. **d**–**f** In contrast, the predictive model IIA maintains stable flocking in over half of the replicas for $\eta \lessapprox 0.225$. Here, **d** polarization gradually decreases from 1, with agents forming V-shaped flocks at zero noise and round flocks at nonzero noise (insets). **e** The average agent-to-center-of-mass distance initially decreases but subsequently increases linearly for $0.015 \lessapprox \eta \lessapprox 0.225$ and coherent replicas, following $\delta_{\mathrm{CM}} \approx (0.35 + 0.19\eta)\zeta$ (inset). **f** The system predominantly consists of a single cluster of communicating agents for $\eta \lessapprox 0.225$, with more than one outlier for $0.015 \lessapprox \eta$ and $0.159 \lessapprox \eta \lessapprox 0.205$. At high noise levels, system size (**b**, **e**) decreases due to the interplay between noise-induced alignment destabilization and suppression of system growth by the diffusive motion of individual subclusters. The models were simulated under the same conditions as in Fig. 2 unless otherwise specified in the figure. The order parameters were evaluated at time $2 \times 10^4 \zeta / v_0$.

doi.org/10.32388/MCG19T.2

The predictive strategies IIA and IIB yield nearly identical results, while strategy IA exhibits slightly better coherence than IB. We attribute this to the slight orientational inertia introduced by the definition of the correlation function in strategies A. In the following, we analyze the behavior of the IIA model under variations in the two key parameters: noise intensity, η, and scaled velocity, v_0/ζ.

With periodic boundary conditions [14], the Vicsek model undergoes a discontinuous phase transition [36] from an ordered to a disordered state. Without periodic boundaries, coherent polarized flocks form only at vanishing noise. When initialized with randomly oriented agents uniformly distributed within a rectangle of side length 4ζ, the model exhibits a monotonic decrease in average polarization (Fig. 3a) and a corresponding increase in the number of communicating clusters (Fig. 3c) as noise intensifies, consistent with this expectation. Notably, the average agent-to-center-of-mass distance reaches a maximum at an intermediate noise level (Fig. 3b). This nonmonotonic behavior arises because, at low noise, the flock expands ballistically, whereas at high noise, the motion of individual subflocks becomes diffusive on the relevant timescale. In this regime, subflocks undergo an effective random walk, slowing the overall expansion of the system.

Under the same conditions and for noise intensities $\eta \lessapprox 0.225$, the predictive model IIA produces coherent flocks consisting of a single cluster of communicating particles (Fig.3f) with polarization $\langle \Phi \rangle \approx 1$ (Fig.3d) in most of the 25 replicas used in our simulations. The inset shows that, in the absence of noise, the coherent flocks adopt a V-shaped formation, reminiscent of those observed in migrating birds, where this arrangement reduces energy expenditure. At nonzero noise levels, the flocks transition to a rounded shape, similar to the formations observed in foraging bird flocks, where cohesion and flexibility are prioritized over aerodynamic efficiency. For videos showing the relaxation of flock shapes and an analysis of the corresponding relaxation times, see the SI [1].

For $\eta \lessapprox 0.015$, the average agent-to-center-of-mass distance decreases with increasing noise. This 'noise stabilization effect' arises from the discrete set of allowed reorientations, which, unlike the classical Vicsek model with arbitrary reorientation per timestep, prevents the system from fully polarizing at zero noise. A similar effect has been observed in Ref. [23]. For $0.015 \lessapprox \eta \lessapprox 0.225$, the average agent-to-center-of-mass distance in stable replicas increases linearly with noise (inset of Fig. 3e). Beyond $\eta \approx 0.225$, all order parameters undergo a transition for the majority of replicas: polarization $\langle \Phi \rangle$ vanishes, δ_{CM} grows by two orders of magnitude within the given simulation time, and the number of clusters approaches the total number of agents. At higher noise levels, both δ_{CM} and the number of clusters slightly decrease, consistent with the diffusive motion of subclusters described above.

doi.org/10.32388/MCG19T.2

In the 25 replicas of the system with different noise realizations obtained from our simulations, a few exceptions to the described behavior appear as empty circles in Fig. 3, representing individual outliers from the typical trend, depicted by the orange lines inside the boxes. The higher number of outliers observed for $\eta \approx 0$ in Fig. 3e, compared to Fig. 3f, arises because each replica contributing to the system size outliers consisted of two separate subflocks, leading to overlapping circles in Fig. 3f. In Sec. S9 [1], we show that the same phenomenology can also be observed when the system is initially perfectly aligned, demonstrating the robustness of the described dynamic phases. For further details on how the described dynamical phases manifest in the behavior of the individual replicas, see Fig. S1 [1].

Role of speed and interaction radius

For a given noise intensity, the system forms a stable flock if the ratio v_0/ζ is small enough so that each agent has sufficient time to align with its neighbors before changing them. In the stable regime, the flock size is proportional to the interaction radius and independent of the speed, i.e., $\delta_{\mathrm{CM}} \sim \zeta_s$. For details, see Fig. S1 [1].

Leadership

In nature, bird flocks often involve a subgroup of leaders who are best informed about the target position and who are followed by the rest of the flock [17][27]. In Fig. S9 and Supplementary video 3 [1], we show that the predictive model IIA can form cohesive flocks also in the scenario when a subgroup of leaders perform an oscillator deterministic motion, albeit for slightly lower v_0/ζ than without the perturbation by leaders.

Discussion

We have presented a cohesive flocking model based solely on alignment interactions, achieved by replacing the Ising-like alignment rule of the Vicsek model with *predictive alignment*, in which agents adopt the predicted prevailing orientation of their future neighbors. For agents unable to predict their future positions, this rule reduces to various modifications of the Vicsek model—since the set of neighbors remains the same for all directions, the magnitude of the mean polarization is independent of the chosen direction. However, agents that can predict the future positions of their neighbors optimize a tradeoff between aligning with neighbors' headings and maintaining proximity, yielding cohesion and order without the need for boundaries or added forces. This approach fundamentally departs from previous models, which rely on such aids [29], and is reminiscent of the reinforcement learning algorithm aimed at minimizing neighbors' losses, as investigated in Refs. [37][38]. From a technical perspective, the dynamical equations feature a reorientation

’force’ that does not follow the gradient of a potential, which would typically lead to stable orientations at local minima. Instead, it is governed by an $\arg\max$ function, which reorients agents toward the deepest minimum of a utility function (negative orientation correlation with neighbors) that is accessible in the next timestep. This process is constrained by the agent’s field of view, reorientation capabilities, and motility.

Our algorithm provides a plausible strategy that intelligent agents with given physical and cognitive abilities might employ to efficiently align with their neighbors. As such, it falls within the class of intrinsically motivated[20][21][22] and cognitive[18][19] active matter algorithms. The algorithm can also be integrated into the broader framework of active inference[39], a general theory of decision-making. However, unlike typical active inference models, our approach does not rely on the assumption that the system state is near the global optimum of a utility function, allowing forces to be described as gradients of generalized potentials. Instead, it enables agents to dynamically adapt the most preferred configuration they perceive.

The model is scalable, and the resulting flock shapes resemble those observed in nature. However, the stationary states predicted by the model are so dense that the average number of neighbors perceived by each agent is significantly higher than the realistic values natural agents are able to process—typically around seven [8]. Moreover, birds have been shown to align with their nearest topological, rather than metric, neighbors [8]. In addition to these issues, future revisions of the model should be accompanied by an analysis of the properties commonly studied in natural flocks or swarms, such as the shapes of correlation functions and their finite-size scaling [40], to allow for a quantitative comparison between natural systems and the model.

Future extensions of the model could investigate modifications to agents’ cognitive abilities—such as enhanced predictive capabilities, perceptual limitations [8], or delays in decision-making processes [41]. Another avenue is to consider agents governed by different physical principles, for example, incorporating inertia or more general non-Markovian effects. Finally, it would be valuable to explore potential applications of models like the one presented here in areas such as swarm robotics [42], where agents are not constrained by biological limitations. Notably, the current approach resembles swarm control algorithms based on individual robot decisions made without explicit information sharing among agents [43].

Supplementary Material

The supplementary information (PDF) is available here.

Statements and Declarations

Acknowledgments

This work is supported and financed by Charles University in Prague, project PRIMUS/22/SCI/009. We acknowledge Klaus Kroy and Maurice Zeuner for their contributions to the initial version of the project, which is summarized in Maurice Zeuner’s bachelor’s thesis, defended at the University of Leipzig in 2020.

Footnotes

[1] See Supplemental Material for definitions of modified variants of the Vicsek model, a discussion of the time- continuous limit of the predictive alignment model, def- initions of order parameters, a discussion of diffusive spreading in the Vicsek model, analyses of replica- resolved behavior and the roles of speed and interaction radius in the predictive alignment model IIA, discussions of flock shapes and leadership, a minimalist variant of the model, an analysis of the independence of results from initial conditions, a proof of scalability, and descriptions of supplementary videos.

References

1. ^*Berg HC, Brown DA (1972). "Chemotaxis in Escherichia coli Analysed by Three-Dimensional Tracking." Nature.* ***239****(5374):500–504. doi:10.1038/239500a0.*
2. ^*Dusenbery DB, Dusenbery PBE (1992). Sensory Ecology: How Organisms Acquire and Respond to Information. W.H. Freeman. https://books.google.cz/books?id=6S1mQgAACAAJ. ISBN 9780716723332.*
3. a, b*Gompper G, Stone HA, Kurzthaler C, Saintillan D, Peruani F, et al. (2025). "The 2025 Motile Active Matter Roadmap." J. Phys.: Condens. Matter.* ***37****(14):143501. doi:10.1088/1361-648X/adac98.*
4. ^*Kaspar C, Ravoo BJ, van der Wiel WG, Wegner SV, Pernice WHP (2021). "The Rise of Intelligent Matter." Nature.* ***594****(7863):345–355. doi:10.1038/s41586-021-03453-y.*
5. a, b, c*Pearce DJG, Miller AM, Rowlands G, Turner MS (2014). "Role of Projection in the Control of Bird Flocks." Proc. Natl. Acad. Sci. U.S.A.* ***111****:10422–10426. doi:10.1073/pnas.1402202111.*
6. ^*Gorbonos D, Ianconescu R, Puckett JG, Ni R, Ouellette NT, et al. (2016). "Long-Range Acoustic Interactions in Insect Swarms: An Adaptive Gravity Model." New J. Phys.* ***18****(7):073042. doi:10.1088/1367-2630/18/7/073042.*
7. ^*Kay RR, Langridge P, Traynor D, Hoeller O (2008). "Changing Directions in the Study of Chemotaxis." Nat Rev Mol Cell Biol.* ***9****(6):455–463. doi:10.1038/nrm2419.*

8. [a, b, c, d, e]*Ballerini M, Cabibbo N, Candelier R, Cavagna A, Cisbani E, et al. (2008). "Interaction Ruling Animal Collective Behavior Depends on Topological Rather Than Metric Distance: Evidence From a Field Study." Proc. Natl. Acad. Sci. U.S.A.* ***105***(4):1232–1237. *doi:10.1073/pnas.0711437105.*
9. ^*Berdahl A, Torney CJ, Ioannou CC, Faria JJ, Couzin ID (2013). "Emergent Sensing of Complex Environments by Mobile Animal Groups." Science.* ***339***(6119):574–576. *doi:10.1126/science.1225883.*
10. ^*Silverberg JL, Bierbaum M, Sethna JP, Cohen I (2013). "Collective Motion of Humans in Mosh and Circle Pits at Heavy Metal Concerts." Phys. Rev. Lett.* ***110***:228701. *doi:10.1103/PhysRevLett.110.228701.*
11. ^*Vicsek T, Zafeiris A (2012). "Collective Motion." Physics Reports.* ***517***(3):71–140. *doi:https://doi.org/10.1016/j.physrep.2012.03.004.*
12. ^*Bechinger C, Di Leonardo R, Löwen H, Reichhardt C, Volpe G, et al. (2016). "Active Particles in Complex and Crowded Environments." Rev. Mod. Phys.* ***88***:045006. *doi:10.1103/RevModPhys.88.045006.*
13. [a, b]*Reynolds CW (1987). "Flocks, Herds and Schools: A Distributed Behavioral Model." ACM SIGGRAPH Comput. Graph.* ***21***:25–34. *doi:10.1145/37402.37406.*
14. [a, b]*Vicsek T, Czirók A, Ben-Jacob E, Cohen I, Shochet O (1995). "Novel Type of Phase Transition in a System of Self-Driven Particles." Phys. Rev. Lett.* ***75***:1226–1229. *doi:10.1103/PhysRevLett.75.1226.*
15. ^*Toner J (2024). The Physics of Flocking: Birth, Death, and Flight in Active Matter. Cambridge University Press. https://books.google.de/books?id=8d8HEQAAQBAJ. ISBN 9781009002394.*
16. ^*Goh S, Westphal E, Winkler RG, Gompper G (2025). "Alignment-Induced Self-Organization of Autonomously Steering Microswimmers: Turbulence, Clusters, Vortices, and Jets." Phys. Rev. Research.* ***7***:013142. *doi:10.1103/PhysRevResearch.7.013142.*
17. [a, b, c]*Couzin ID, Krause J, Franks NR, Levin SA (2005). "Effective Leadership and Decision-Making in Animal Groups on the Move." Nature.* ***433***:513–516. *doi:10.1038/nature03236.*
18. [a, b, c]*Barberis L, Peruani F (2016). "Large-Scale Patterns in a Minimal Cognitive Flocking Model: Incidental Leaders, Nematic Patterns, and Aggregates." Phys. Rev. Lett.* ***117***:248001. *doi:10.1103/PhysRevLett.117.248001.*
19. [a, b, c]*Lavergne FA, Wendehenne H, Bäuerle T, Bechinger C (2019). "Group Formation and Cohesion of Active Particles With Visual Perception–Dependent Motility." Science.* ***364***:70–74. *doi:10.1126/science.aau5347.*
20. [a, b]*Moussaïd M, Helbing D, Theraulaz G (2011). "How Simple Rules Determine Pedestrian Behavior and Crowd Disasters." Proc. Natl. Acad. Sci. U.S.A.* ***108***:6884–6888. *doi:10.1073/pnas.1016507108.*
21. [a, b]*Romanczuk P, Couzin ID, Schimansky-Geier L (2009). "Collective Motion Due to Individual Escape and Pursuit Response." Phys. Rev. Lett.* ***102***:010602. *doi:10.1103/PhysRevLett.102.010602.*
22. [a, b, c]*Charlesworth HJ, Turner MS (2019). "Intrinsically Motivated Collective Motion." Proc. Natl. Acad. Sci. U.S.A.* ***116***:15362–15367. *doi:10.1073/pnas.1822069116.*

23. ^a, b, c^ *Devereux HL, Turner MS (2023). "Environmental Path-Entropy and Collective Motion." Phys. Rev. Lett. **130**: 168201. doi:10.1103/PhysRevLett.130.168201.*
24. ^ *Ito S, Uchida N (2024). "Selective Decision-Making and Collective Behavior of Fish by the Motion of Visual Attention." PNAS Nexus. **3**(7):pgae264. doi:10.1093/pnasnexus/pgae264.*
25. ^ *Castro D, Eloy C, Ruffier F (2025). "Visual Collective Behaviors on Spherical Robots." Bioinspir. Biomim. **20**(2):026006. doi:10.1088/1748-3190/adaab9. PMID 39813794.*
26. ^ *Ashraf I, Bradshaw H, Ha TT, Halloy J, Godoy-Diana R, et al. (2017). "Simple Phalanx Pattern Leads to Energy Saving in Cohesive Fish Schooling." Proc. Natl. Acad. Sci. U.S.A. **114**:9599–9604. doi:10.1073/pnas.1706503114.*
27. ^a, b^ *Nagy M, Ákos Z, Biro D, Vicsek T (2010). "Hierarchical Group Dynamics in Pigeon Flocks." Nature. **464**:890–893. doi:10.1038/nature08891.*
28. ^ *Virágh C, Vásárhelyi G, Tarcai N, Szörényi T, Somorjai G, et al. (2014). "Flocking Algorithm for Autonomous Flying Robots." Bioinspir. Biomim. **9**:025012. doi:10.1088/1748-3182/9/2/025012.*
29. ^a, b, c^ *Chaté H, Ginelli F, Grégoire G, Peruani F, Raynaud F (2008). "Modeling Collective Motion: Variations on the Vicsek Model." Eur. Phys. J. B. **64**:451–456. doi:10.1140/epjb/e2008-00275-9.*
30. ^a, b^ *Solon AP, Caussin JB, Bartolo D, Chaté H, Tailleur J (2015). "Pattern Formation in Flocking Models: A Hydrodynamic Description." Phys. Rev. E. **92**:062111. doi:10.1103/PhysRevE.92.062111.*
31. ^ *Nagy M, Daruka I, Vicsek T (2007). "New Aspects of the Continuous Phase Transition in the Scalar Noise Model (SNM) of Collective Motion." Physica A: Stat. Mech. Appl. **373**:445–454. doi:10.1016/j.physa.2006.05.035.*
32. ^ *González-Albaladejo R, Carpio A, Bonilla LL (2023). "Scale-Free Chaos in the Confined Vicsek Flocking Model." Phys. Rev. E. **107**:014209. doi:10.1103/PhysRevE.107.014209.*
33. ^ *Caprini L, Löwen H (2023). "Flocking Without Alignment Interactions in Attractive Active Brownian Particles." Phys. Rev. Lett. **130**:148202. doi:10.1103/PhysRevLett.130.148202.*
34. ^ *Rendell L, Boyd R, Cownden D, Enquist M, Eriksson K, et al. (2010). "Why Copy Others? Insights From the Social Learning Strategies Tournament." Science. **328**:208–213. doi:10.1126/science.1184719.*
35. ^ *Ginelli F (2016). "The Physics of the Vicsek Model." Eur. Phys. J. Spec. Top. **225**:2099–2117. doi:10.1140/epjst/e2016-60066-8.*
36. ^ *Chaté H, Ginelli F, Grégoire G, Raynaud F (2008). "Collective Motion of Self-Propelled Particles Interacting Without Cohesion." Phys. Rev. E. **77**:046113. doi:10.1103/PhysRevE.77.046113.*
37. ^ *Durve M, Peruani F, Celani A (2020). "Learning to Flock Through Reinforcement." Phys. Rev. E. **102**:012601. doi:10.1103/PhysRevE.102.012601.*
38. ^ *Brambati M, Celani A, Gherardi M, Ginelli F (2025). "Learning to Flock in Open Space by Avoiding Collisions and Staying Together." https://arxiv.org/abs/2506.15587.*

39. ^Parr T, Pezzulo G, Friston KJ (2022). *Active Inference: The Free Energy Principle in Mind, Brain, and Behavior.* The MIT Press. doi:10.7551/mitpress/12441.001.0001. ISBN 9780262369978.
40. ^Cavagna A, Giardina I, Grigera TS (2018). *"The Physics of Flocking: Correlation as a Compass From Experiments to Theory." Physics Reports.* **728**:1–62. doi:10.1016/j.physrep.2017.11.003.
41. ^Holubec V, Geiss D, Loos SAM, Kroy K, Cichos F (2021). *"Finite-Size Scaling at the Edge of Disorder in a Time-Delay Vicsek Model." Phys. Rev. Lett.* **127**:258001. doi:10.1103/PhysRevLett.127.258001.
42. ^Hamann H (2018). *Swarm Robotics: A Formal Approach. Springer International Publishing.* https://books.google.de/books?id=pnNLDwAAQBAJ. ISBN 9783319745282.
43. ^Bayındır L (2016). *"A Review of Swarm Robotics Tasks." Neurocomputing.* **172**:292–321. doi:10.1016/j.neucom.2015.05.116.

Supplementary data: available at https://doi.org/10.32388/MCG19T.2

Declarations

Funding: This work is supported and financed by Charles University in Prague, project PRIMUS/22/SCI/009.

Potential competing interests: No potential competing interests to declare.